Using NOAA Satellite Imagery to Detect and Track Hazardous Sea Spray in the High Latitudes

WILLIAM E. LINE,[a] LEWIS GRASSO,[b] DON HILLGER,[a] CARL DIERKING,[c] AARON JACOBS,[d] AND SAMUEL SHEA[e]

[a] *NOAA/NESDIS/Center for Satellite Applications and Research/Regional and Mesoscale Meteorology Branch, Fort Collins, Colorado*
[b] *Cooperative Institute for Research in the Atmosphere, Colorado State University, Fort Collins, Colorado*
[c] *Geographic Information Network of Alaska, University of Alaska Fairbanks, Fairbanks, Alaska*
[d] *NOAA/National Weather Service, Juneau, Alaska*
[e] *NOAA/National Weather Service, Anchorage, Alaska*

(Manuscript received 19 August 2021, in final form 3 January 2022)

ABSTRACT: Sea spray presents a significant hazard to vessels in the high latitudes. At issue is the accumulation of ice, which can destabilize, and at times, sink a ship. Many studies have focused on icing prediction systems, but a knowledge gap exists in the detection of sea spray using remote sensing data. The recent availability of data from new and advanced imagers on board NOAA satellites, specifically the GOES-R series Advanced Baseline Imager (ABI) and JPSS Visible Infrared Imaging Radiometer Suite (VIIRS), offers new tools for the detection and tracking of sea spray for forecasters. While ABI provides superior temporal coverage in order to capture the near-real-time evolution of sea spray, VIIRS contributes higher spatial detail, allowing for improved analysis of sea spray extent, particularly within smaller bodies of water. Forecasters can implement these detection techniques to help verify sea spray–related forecast products, and to pass along potentially life-saving information to their mariner core partners. This paper discusses the freezing sea spray hazard, and introduces newly identified methods for detecting and tracking sea spray using NOAA satellite data.

KEYWORDS: Satellite observations; Operational forecasting; Decision support; Aerosols/particulates; Air-sea interaction

1. Introduction

Oceanic whitecaps develop as a result of wave breaking and subsequent entrainment of air into the ocean, forming bubbles and seafoam just below and on the ocean surface, respectively (Salisbury et al. 2013). The subsequent popping of whitecap bubbles releases aerosols (film and jet droplets) into the atmosphere immediately above the ocean surface, known as sea spray (Blanchard 1983; Wu 1992; Anguelova and Webster 2006). Sea spray also develops as a result of strong winds separating aerosols from the wave crest (spume droplets) and distributing them into the atmosphere (Andreas et al. 1995). Larger sea spray aerosols (SSA; from 10 nm to several millimeters) can remain suspended in the air for seconds to minutes, while smaller particles can reside in the air for days (De Leeuw et al. 2011).

For the past several decades, the influence of sea spray on tropical and midlatitude cyclone morphology has been an active area of research. Herbert Riehl is credited as the first person to point out the important role sea spray may have on tropical cyclone morphology (Riehl 1954). Subsequent studies have focused on the impact of sea spray on tropical cyclone structure and intensity through laboratory experiments and numerical models (Ortiz-Suslow et al. 2016; Rastigejev and Suslov 2014; Gall et al. 2008; Wang et al. 2001; Andreas and Emanuel 2001; Fairall et al. 1994; Andreas and DeCosmo 1999). Efforts have also been given to understanding the role of sea spray on midlatitude cyclones (Perrie et al. 2005; Zhang et al. 2006; Meirink and Makin 2001).

Sea spray also presents a significant hazard to vessels in the high latitudes. At issue is the accumulation of ice, which can destabilize, and at times, sink a ship (Shellard 1974; Panov 1978; Dehghani-Sanij et al. 2017). Recently, two vessels were lost in which icing played a role: 1) the 110-ft crabber *Destination*, which sank February 2017 northwest of St. George Island, Alaska; and 2) the 130-ft *Scandies Rose*, which sank December 2019 near Kodiak, Alaska (Moore 2020). Many studies have focused on vessel icing prediction systems (Lozowski et al. 2000; Samuelson et al. 2015; Jones and Andreas 2012). Prediction of icing of vessels is a complicated effort since icing of such sea-born structures is a function of the 1) size of a vessel, relative to the wavelength of ocean waves; 2) bearings of a vessel, relative to the prevailing wind; 3) ambient wind speed; 4) air temperature; 5) sea temperature; and 6) geometry of a given vessel (Makkonen et al. 1991; Overland 1990; Overland et al. 1986). More specifically regarding the environmental conditions, vessel icing can occur in the presence of wind speeds over 18 kt (9 m s^{-1}), air temperatures below −1.7°C, and sea temperature below 7°C (Guest and Luke 2005).

The National Weather Service (NWS) issues a Coastal Waters Forecast (CWF) that will include a mention of "freezing

Denotes content that is immediately available upon publication as open access.

Supplemental information related to this paper is available at the Journals Online website: https://doi.org/10.1175/WAF-D-21-0137.s1.

Corresponding author: William E. Line, bill.line@noaa.gov

DOI: 10.1175/WAF-D-21-0137.1

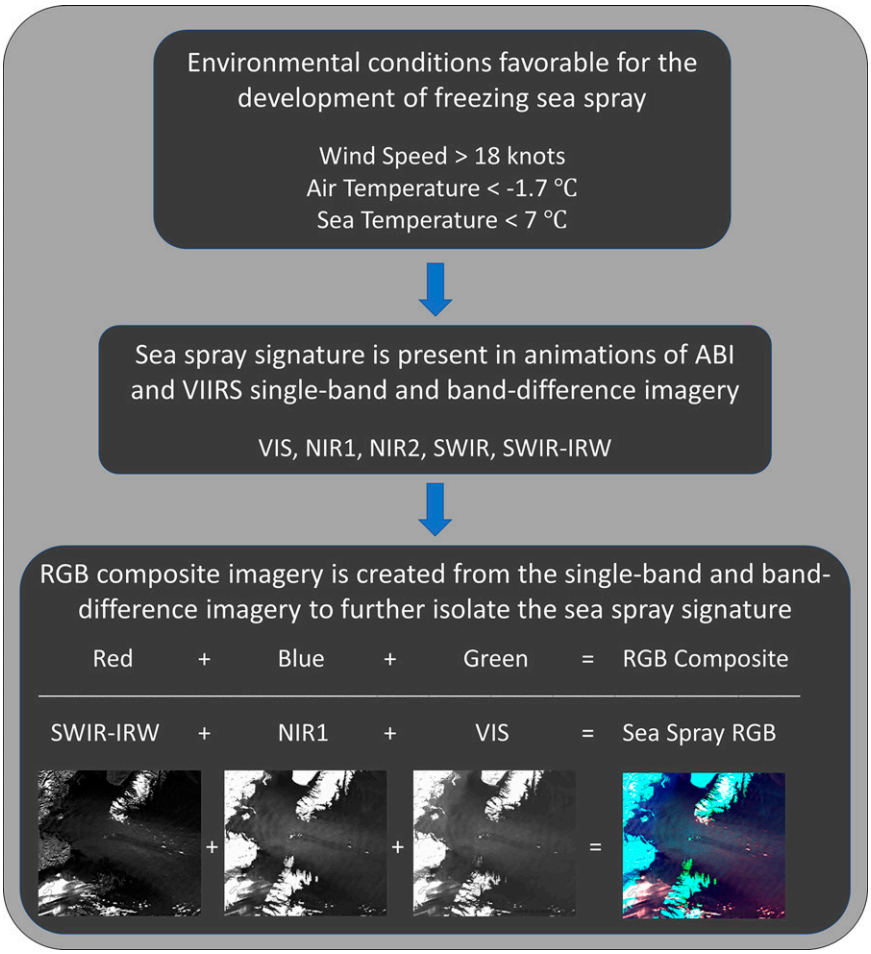

FIG. 1. Flowchart summarizing the environmental conditions conducive to the development of freezing sea spray and the process for how sea spray is detected using NOAA satellite imagery.

spray" if the appropriate combination of environmental conditions are forecast to result in an accumulation of freezing water droplets on a vessel. A "heavy freezing spray warning" will be included in the forecast if conditions are expected to result in an accumulation of freezing water droplets on a vessel at a rate of 2 cm h^{-1} or greater (NWS 2020). Additionally, forecasters will inform relevant mariners of the potential for freezing spray via informal briefings, a method of Impact-based Decision Support Services (IDSS). Unfortunately, observations of sea spray in the high latitudes are scarce. At NWS Weather Forecast Office (WFO) Anchorage, Alaska, freezing spray is one of the warnings that is rarely verified. Therefore, additional confirmation of ongoing sea spray would be beneficial to high-latitude forecasters in verifying forecast and warning products, and providing more effective IDSS to interested partners.

This paper will serve as an initial analysis into sea spray detection capabilities over Alaska area waters, where freezing spray may result, leveraging National Oceanic and Atmospheric Administration (NOAA) operational weather satellite imagery currently available to NWS forecasters. Herein are some of the first documented clear-sky observations of sea spray at high latitudes from NOAA operational satellites. The first section will introduce the satellite imagery utilized to observe sea spray over Alaska waters, collected from instruments aboard *Geostationary Observational Environmental Satellite* (*GOES-17*), *Suomi National Polar-Orbiting Partnership* (*SNPP*), and *NOAA-20*. The paper will then highlight the satellite detection techniques used to diagnose sea spray, along with a demonstration by way of two cases. Initial focus is given to a region over southwest Alaska between the Kodiak archipelago and Kenai Peninsula. This region has been the subject of meteorological studies due to a boundary layer jet that develops from Kamishak Bay, Alaska, southeast over lower portions of Cook Inlet, over the Barren Islands, southeastward to northern portions of the Gulf of Alaska (GoA; Liu et al. 2006; Macklin et al. 1990). The second case takes place within the inner channels of southeast Alaska, representing smaller-scale bodies of water often subject to strong winds and freezing spray events. These case studies will be followed by a discussion on the relevancy of sea spray detection to the NWS, and a conclusion summarizing key findings and ideas for future work.

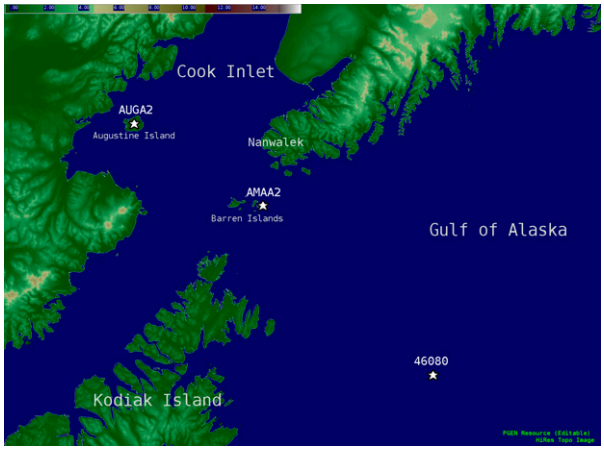

FIG. 2. Region of interest for the 10 Feb 2020 sea spray case. Relevant geographic landmarks (gray) and locations of C-Man stations and buoys (white) are labeled.

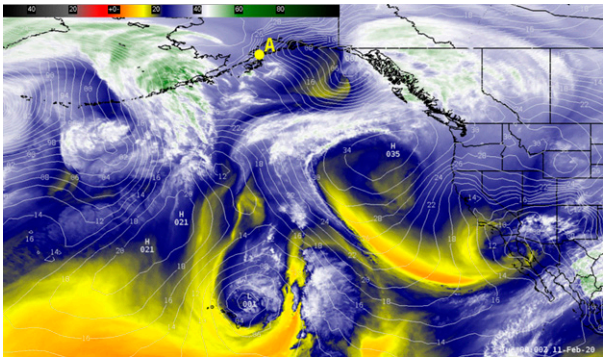

FIG. 3. The 0000 UTC 11 Feb 2020 GOES-West 6.2-μm water vapor imagery (color fill) and GFS mean sea level pressure analysis (hPa; white contours). Point A refers to the region of interest for this case.

2. Satellite data and display

The Visible Infrared Imaging Radiometer Suite (VIIRS) instrument is available on the *SNPP* and *NOAA-20* satellites, which are part of the Joint Polar Satellite System (JPSS; Goldberg et al. 2013; Hillger et al. 2013). *SNPP* and *NOAA-20* are in early afternoon sun-synchronous orbits separated by one-half orbit, resulting in 50 min between two VIIRS images over a given location at approximately the same time each day and night. Near the southern Alaskan coast and within the GoA, considering overlap, a given location can expect to be included in 4–6 *SNPP* plus *NOAA-20* VIIRS swaths during the early afternoon and again at night. VIIRS allows for imaging of sub-satellite footprints at both 750 m (M-band imagery) and 375 m (I-band imagery). In this paper, analysis will be focused on the five 375-m I bands in order to capture the sea spray signature at higher resolution, and for comparison with similar wavelength but lower resolution GOES bands. The central wavelengths of the I bands 1–5 are 0.64, 0.865, 1.61, 3.74, and 11.45 μm, respectively.

GOES-17, or GOES-West, provides geostationary satellite coverage across the eastern Pacific Ocean and western North America from 137.2°W. One of the Earth-pointing instruments on board *GOES-17* is the Advanced Baseline Imager (ABI), which represents a significant advancement over imagers on previous generation GOES satellites (Schmit et al. 2017). ABI collects imagery at 16 different spectral bands with a spatial resolution at nadir, depending on band, of 0.5, 1, and 2 km. *GOES-17* has operated in 10-min Flex Mode (Mode 6) as the primary operating mode since 2 April 2019, which collects full disk (full hemisphere) imagery every 10 min, Pacific United States (PACUS) imagery every 5 min, and two moveable 1000 km $\times$ 1000 km "mesoscale sectors" of 1-min imagery each, or one such sector of 30-s imagery (Schmit and Gunshor 2020).

The GOES-West 5-min PACUS sector does not include Alaska and surrounding waters. While the default position of GOES-West mesoscale sector 2 is positioned over part of Alaska, it includes a limited geographic area, and is often scanning elsewhere upon request. Therefore, this study will evaluate the routinely available GOES-West 10-min full disk imagery, which always includes all of Alaska and surrounding waters. Given the high latitude of the GoA and southern Alaskan shores, ABI imagery spatial resolution is degraded, with an approximate pixel area 3–4 times larger than that at satellite nadir (Schmit et al. 2017). For example, GOES-West band 5, which has a pixel resolution of 1 km at nadir, has an approximate pixel resolution of 3–4 km over Cook Inlet. In this study, analysis will be performed on ABI bands 2, 3, 5, 7, 13 only, closely matching the spectral bands available from the VIIRS I-bands already introduced. The central wavelengths (spatial resolutions at nadir) of the five aforementioned ABI bands are 0.64 μm (0.5 km), 0.865 μm (1 km),

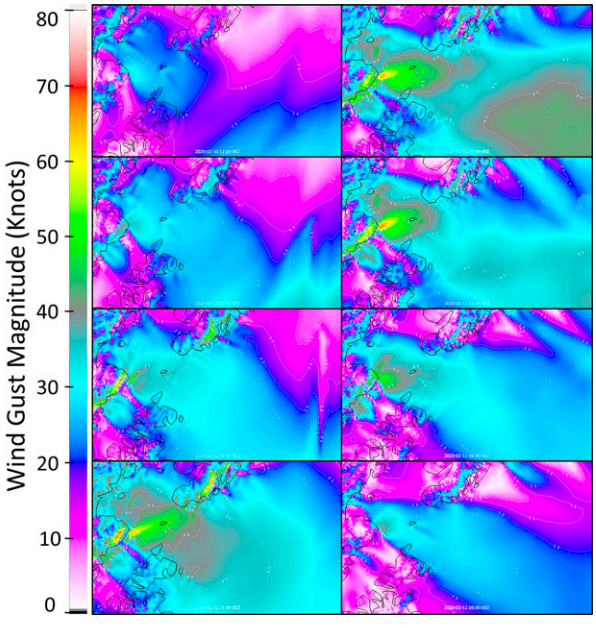

FIG. 4. The 1200 UTC 10 Feb–0900 UTC 11 Feb 2020 NCEP/HRRR 3-hourly (shown from top to bottom and from left to right) wind gust (kt) analysis fields (fill and contour).

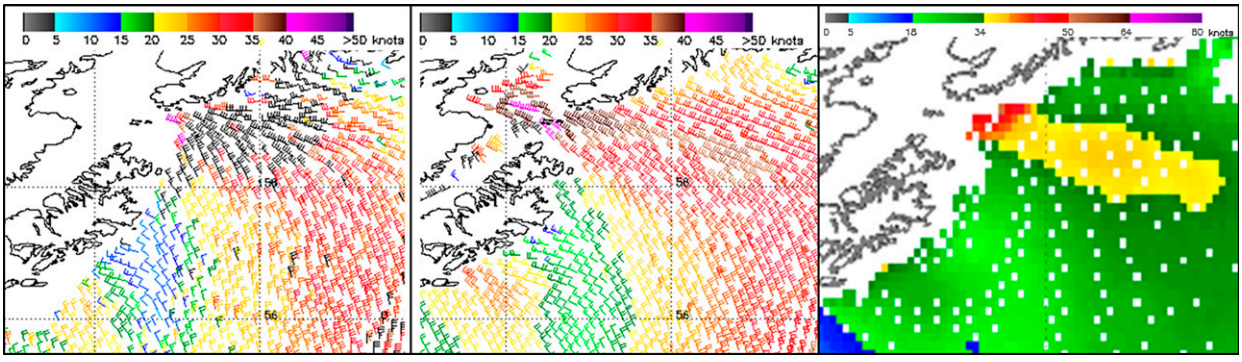

FIG. 5. The 10 Feb 2020 (left) SCATSAT (2000 UTC) and (center) *MetOp-B* ASCAT (2115 UTC) wind barbs (kt), and (right) AMSR-2 (2250 UTC) wind speeds (kt).

1.61 μm (1 km), 3.90 μm (2 km), and 10.35 μm (2 km), respectively. Herein, the five corresponding ABI and VIIRS bands will be referred to as visible (VIS), near-infrared 1 (NIR1), near-infrared 2 (NIR2), shortwave-infrared (SWIR), and infrared-window (IRW), respectively.

Due to a relative lack of ground truth verification, very high-resolution imagery collected by the European Space Agency (ESA) Sentinel-2 mission satellites was utilized to confirm the presence of sea spray in suspected regions based on signatures in ABI and VIIRS imagery (Drusch et al. 2012). The Sentinel-2 mission consists of two identical satellites, *Sentinel-2A* and *Sentinel-2B*, that each carry a single instrument: the Multi-Spectral Instrument (MSI). MSI collects 10-m resolution imagery at visible wavelengths (blue, green, red), allowing for the creation of 10-m true color imagery used in this paper. At 10-m resolution, individual whitecaps and associated sea spray can be resolved in true color imagery. A given location over the GoA and surrounding coastal areas will experience a Sentinel-2 pass with a consistent viewing angle once every 5 days, with overlap between swaths allowing for an additional 1–2 passes of varying viewing angles within that time period. Therefore, while the spatial resolution is ideal for detecting small-scale phenomena, the temporal coverage and availability of the Sentinel-2 mission over a given point is not sufficient for real-time operational use.

To display the ABI and VIIRS imagery, this study utilized the Advanced Weather Interactive Processing System II (AWIPS-II) and the Man computer Interactive Data Access System-V (McIDAS-V). AWIPS-II is the software utilized by the NWS for meteorological data visualization and forecast product generation. McIDAS-V is a software package developed at the Space Science and Engineering Center in Madison, Wisconsin, that provides an alternative means for visualizing meteorological data, most notably satellite imagery and products (Achtor et al. 2008). ABI and VIIRS data were procured at the Cooperative Institute for Research in the Atmosphere (CIRA) via the Satellite Broadcast Network, and from the NOAA Comprehensive Large Array-Data Stewardship System (CLASS).

3. Sea spray identification techniques

a. Physical basis for sea spray appearance in NOAA satellite imagery

Figure 1 summarizes the detection of sea spray using NOAA satellite imagery as introduced in this paper. Discussing the various bands in an instrument-agnostic sense, in the

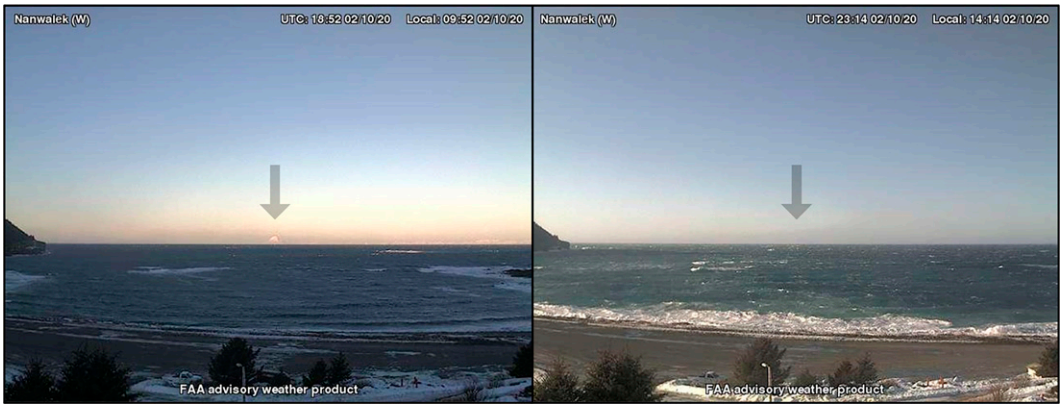

FIG. 6. The (left) 1852 and (right) 2314 UTC FAA webcam at Nanwalek, looking west toward Augustine Island in Cook Inlet. Augustine Island (marked by arrow) can be found in the left image, but is masked by haze in the right image.

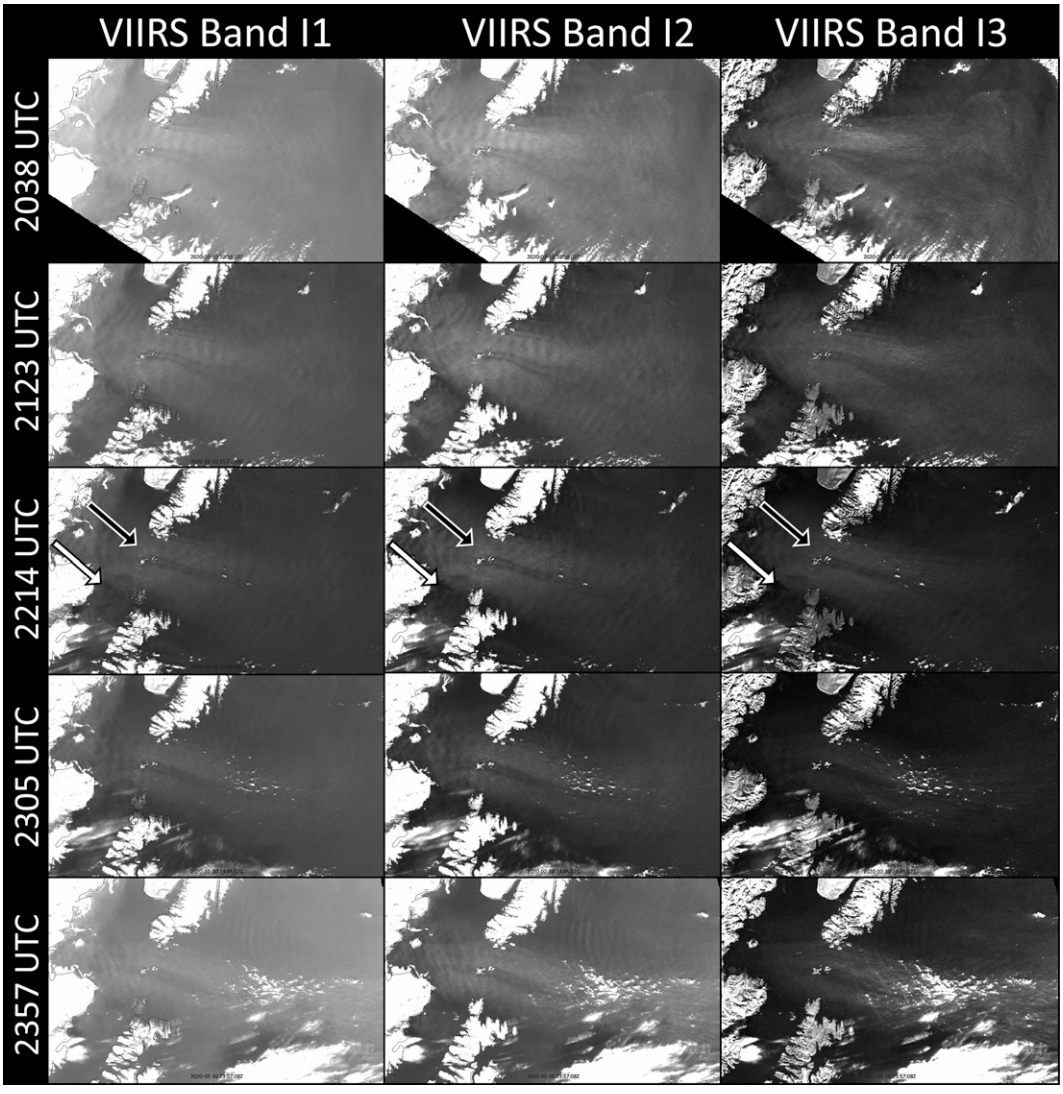

FIG. 7. The 2038, 2123, 2214, 2305, and 2357 UTC (shown from top to bottom) 10 Feb 2020 *NOAA-20* and *SNPP* VIIRS bands (left) I1, (center), I2, and (right) I3 (see text for wavelength associations). All products utilize a linear grayscale color table, with increasing reflectance represented by increasingly lighter shades of gray. Arrows point to areas of sea spray (black with white outline) and non–sea spray (white with black outline).

VIS and NIR bands, the sea spray signature is represented as a region of relatively high albedo compared to the surrounding clear-sky areas. The high albedo signature is due to scattering of solar radiation by the suspended SSA. The sea spray signature is more apparent in the longer wavelength NIR bands compared to the VIS band given their 1) lower sensitivity to scattering by additional smaller atmospheric aerosols adjacent to and above the SSA, and 2) lower reflectance off of turbid waters. These characteristics allow the two NIR bands to sense boundary layer phenomena with minor atmospheric contamination and with high contrast between the SSA and adjacent clear skies and clear waters.

The SWIR band includes contributions from both reflected solar radiation and emitted terrestrial radiation. The sea spray signature exhibits slightly warmer brightness temperatures compared to other areas due to the extra contribution of scattering by the SSA. There is no sea spray brightness temperature signature in the IRW. By differencing the SWIR and IRW bands, therefore, the result is a reflected (solar) component. Sea spray appears as a positive difference in the SWIR minus IRW band difference (SWIR-IRW), since scattering of solar energy by the SSA is acting to increase the brightness temperature in the SWIR above what is observed in the IRW.

b. Methods used to detect sea spray in NOAA satellite imagery

Various color tables and data ranges were developed and tested with the single-band and band-difference imagery for the cases discussed in order to best highlight the sea spray. A linear grayscale color table applied to both ABI and VIIRS

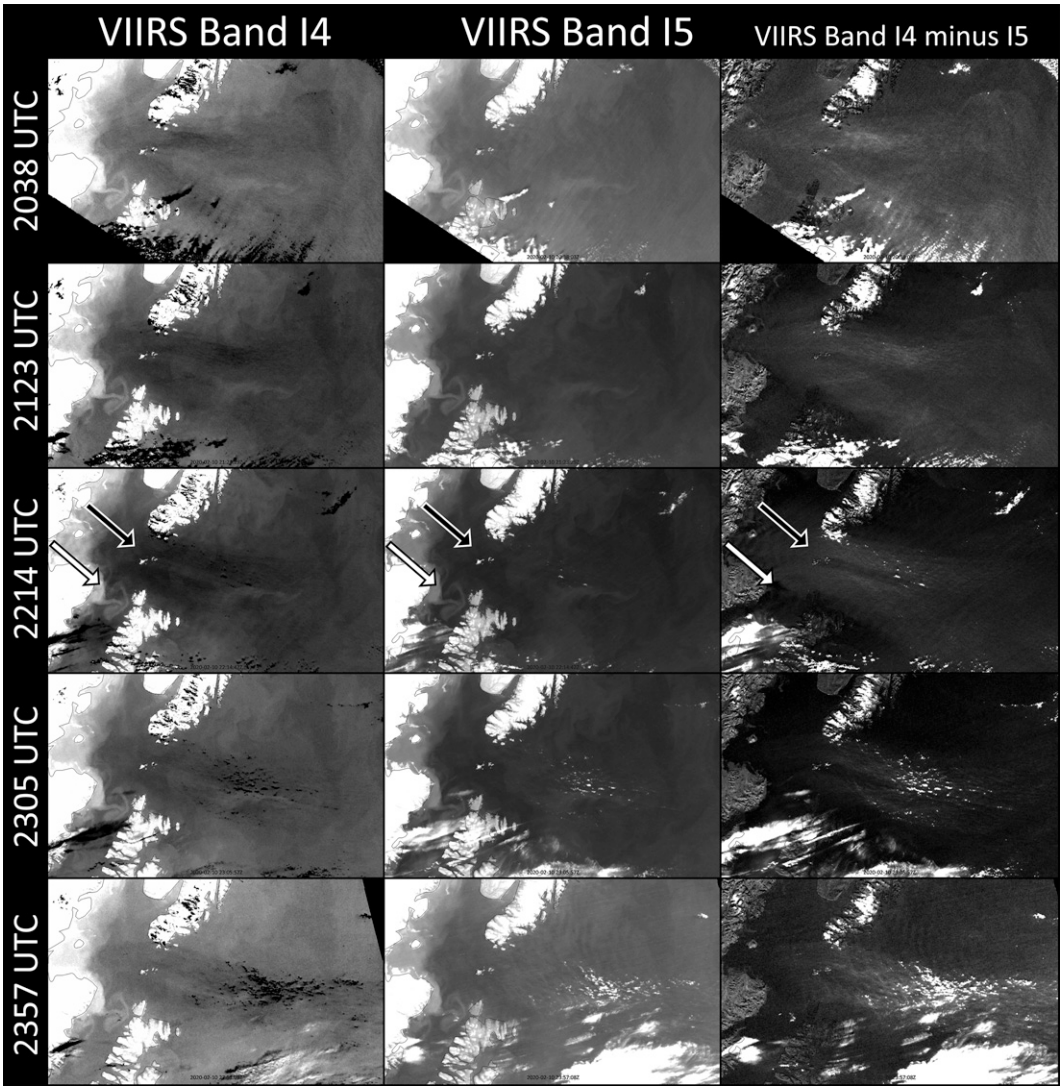

FIG. 8. The 2038, 2123, 2214, 2306, and 2357 UTC (shown from top to bottom) 10 Feb 2020 *NOAA-20* and *SNPP* VIIRS bands (left) I4, (center) I5, and (right) I4 minus I5 difference (see text for wavelength associations). All products utilize a linear grayscale color table, with decreasing brightness temperature/increasing difference represented by increasingly lighter shades of gray. Arrows point to areas of sea spray (black with white outline) and non–sea spray (white with black outline).

imagery appeared to provide the right balance between: 1) capturing a sea spray signature and 2) adaptability to varying situations, primarily related to differing viewing and sun angles. Color table ranges were set for each unique band and band difference in an effort to best highlight the sea spray feature for these cases. The chosen color table ranges vary from band to band given feature sensitivity differences, from ABI to VIIRS given viewing angle differences, and from case to case given sun angle differences. Changes to the color table range are simple and quick to complete in real time in NWS AWIPS-II, and are recommended in order to best highlight the feature considering the aforementioned variables. Given the simplicity of the linear grayscale color table, value range changes can be made at will without fear of disrupting a color pattern.

RGB composites combine the benefits of up to three satellite bands or band differences into a single image (EUMETSAT User Services 2009). In this study, unique RGB composites were created for both ABI and VIIRS imagery in an effort to capture and isolate sea spray across a range of events within a single product. The red, green, and blue components of the sea spray RGB are the SWIR-IRW, NIR1 band, and VIS band, respectively. These bands were chosen because they are available from both ABI and VIIRS, and contribute to sea spray detection. While, with VIIRS, all chosen bands are 375-m resolution, with ABI, the VIS band provides 4 times better resolution than the NIR bands, and 16 times that of the SWIR and IRW bands. The higher spatial resolution allows for more precise detection of sea spray initiation and plume edges, as well as

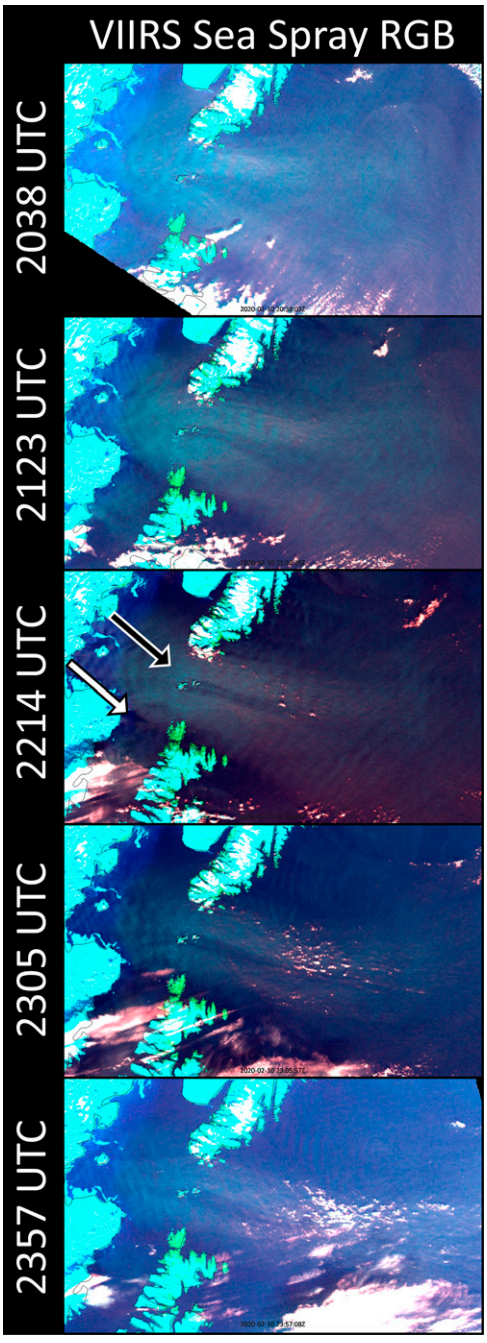

FIG. 9. The 2038, 2123, 2214, 2306, and 2357 UTC 10 Feb 2020 *NOAA-20* and *SNPP* VIIRS sea spray RGB (shown from top to bottom). Details about the sea spray RGB can be found in the text. Arrows point to areas of sea spray (black with white outline) and non–sea spray (white with black outline).

smaller- and weaker-scale sea spray events. That, along with its greater sensitivity to aerosol scattering, makes the VIS band valuable in the ABI sea spray RGB. The inclusion of the NIR1 band provides slightly better contrast between sea spray areas and non–sea spray areas compared to the VIS and NIR2 bands. The SWIR-IRW was chosen, despite slightly lower spatial resolution with ABI, to further highlight the sea spray signature, while also masking out clouds. Despite being sensed in the VIS band, the lack of sensitivity to turbid waters in the NIR1 and SWIR-IRW allow it to be differentiated from the sea spray. The RGBs can be installed in AWIPS locally for both VIIRS and ABI using existing data and capabilities, negating the need for additional data delivery and software.

Sea spray detection using NOAA satellite imagery is most effective when the user analyzes the aforementioned single-band and/or multispectral images as animations. While the feature can be diagnosed within a single image, the viewing of successive images introduces another dimension to the imagery that improves overall understanding of the scene. This method of imagery analysis is commonplace for operational forecasters in order to identify a given atmospheric feature or trend (Line et al. 2016; Lindley et al. 2016; Elsenheimer and Gravelle 2019).

c. *Considerations when using NOAA satellite imagery to detect sea spray*

While this paper focuses on the detection of sea spray using NOAA Satellites, there are a few considerations to remember when using these techniques to diagnose areas of sea spray and potential freezing spray. Given the sea spray detection technique utilizes visible, near-infrared, and infrared bands aboard satellites, and the sea spray phenomenon occurs near the surface, clear-sky conditions are required. Next, while sea spray is confirmed with the cases discussed herein, the satellite signature introduced in this paper may result from a small contribution of reflectance off of active whitecaps on the ocean surface, in addition to scattering by SSA. Although it is difficult to separate the two contributions with NOAA satellite capabilities, previous research suggests whitecaps represent areas of active sea spray production (Anguelova and Webster 2006). Therefore, a contribution to the signal from the ocean surface would itself imply the generation of sea spray. Additionally, during certain times of year, sun glint off of the sea surface may temporarily diminish the user's ability to diagnose sea spray. This influence would be temporary (up to a few frames), allowing the user to still diagnose the signature in prior and subsequent frames. On another note, the collision of waves on a marine vessel within the active sea spray region may result in additional sea spray generation and marine icing (Overland et al. 1986; Dehghani-Sanij et al. 2017). Finally, the sea spray signature does not necessarily mean freezing spray is occurring. Air and ocean temperature along with vessel characteristics need to meet thresholds for the generation of freezing sea spray, as discussed in section 1.

4. Case studies

Two recent freezing spray events will be analyzed in this study. These are two of the first cases in which the authors noted the appearance of sea spray in NOAA satellite imagery, and where sea spray could be confirmed by other sources. The first case from 10 February 2020 will focus on a large-

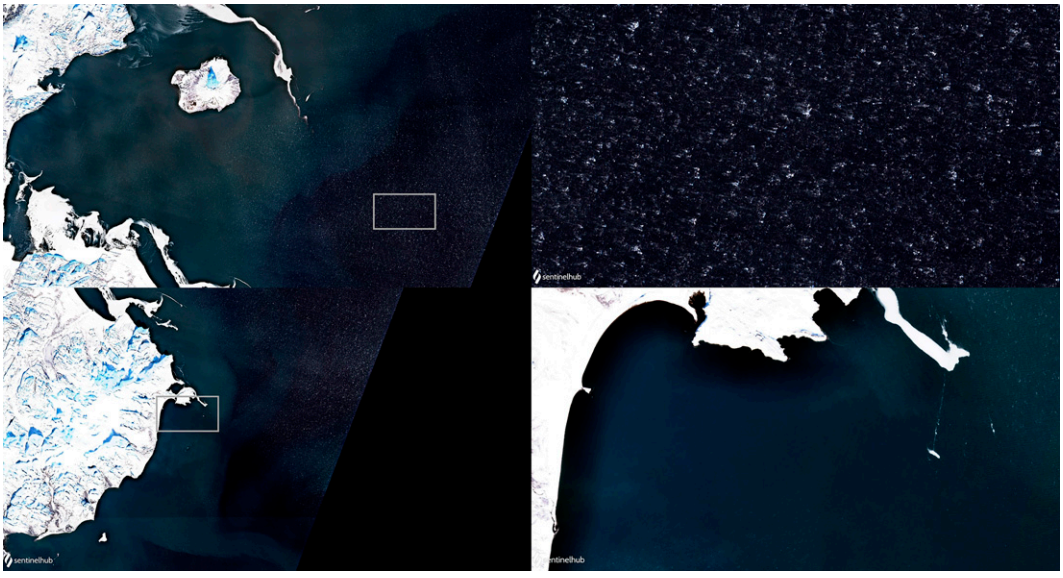

FIG. 10. The 2149 UTC 10 Feb 2020 Sentinel-2 true color imagery. Imagery is from portions of Cook Inlet. The gray rectangles in the left images denote the zoomed in regions of the right images.

scale sea spray event developing across Cook Inlet and into the adjacent open GoA. The second case will focus on a 5 March 2020 smaller-scale sea spray event taking place within the inner channels of southeast Alaska near Juneau. Sea spray will be analyzed using imagery from GOES-West ABI, *Suomi NPP*, and *NOAA-20* VIIRS, and Sentinel-2 MSI. Sectors containing both sea spray and calm waters will be studied for comparison. Buoy observations, surface webcams, and photographs will be shown, where available, to confirm the presence of sea spray and favorable environmental conditions for freezing spray. NWS text forecast products including the mention of freezing spray will also be shared. Given the relative lack of surface wind observations spatially, 3-hourly National Centers for Environmental Prediction (NCEP)/High Resolution Rapid Refresh (HRRR)–Alaska model analyses will also be shown to represent the extent of strong wind gusts.

a. 10 February 2020 Cook Inlet case study

Strong gusty winds developed across Cook Inlet and the broader GoA during the day on 10 February 2020 on the backside of a low pressure system (Fig. 2). GOES-West full disk water vapor imagery depicted the upper-level shortwave trough accelerating through the eastern portion of the GoA, while another shortwave trough approached from the west, with a shortwave ridge between the features spanning the western GoA and Cook Inlet (Fig. 3). At the surface, GFS model analyses indicated low pressure associated with the lead shortwave was centered over the eastern GoA by 1800 UTC, with a tight surface pressure gradient on the backside of the low still present over western portions of the GoA. This pattern resulted in cold air advection over the area of interest, ushering in the cold air and gusty winds necessary for the development of freezing spray. Given the environmental conditions, the Anchorage, Alaska, NWS WFO issued a CWF at 0314 local time (LT) that included mention of "freezing spray" during the day and evening across much of Cook Inlet and into the western GoA, and a heavy freezing spray warning during the evening for much of Cook Inlet. Specifically, the NWS forecast during the day and early evening included wind speeds to 45 kt (23 m s^{-1}) and wave heights to 14 ft (4 m).

The setup did result in strong westerly winds channeling through the Kamishak Gap and extending east across southern portions of Cook Inlet and the Barren Islands, and into western portions of the GoA. HRRR model analyses from the region included a wide swath of 30–40 kt (15–21 m s^{-1}) wind gusts first developing within Cook Inlet by 1800 UTC, increasing to 35–50 kt (18–26 m s^{-1}) and extending east into the western GoA thereafter through 0300 UTC, before subsiding again (Fig. 4). Satellite-based instruments, including SCATSAT (2000 UTC), *MetOp-B* ASCAT (2115 UTC), and AMSR-2 (2250 UTC), measured a swath of wind speeds as high as 35–45 kt (18–23 m s^{-1}) extending from southern Cook Inlet east into the western GoA (Fig. 5).

C-Man station and buoy observations available over the same region confirm the temporal trends of meteorological conditions necessary for the development of sea spray and freezing spray throughout the day. Sustained wind speeds and wind gusts of 18–36 kt (9–19 m s^{-1}) and 25–46 kt (13–24 m s^{-1}), respectively, were observed at AUGA2, and 10–28 kt (5–14 m s^{-1}) and 18–50 kt (9–26 m s^{-1}), respectively, at AMAA2, during the daytime period of 1800 and 0200 UTC. Air temperatures ranged from −7.0° to −10.7°C and from −2.2° to −5.7°C during the same period at the two sites, respectively. Buoy station 46080 measured wave heights in the 2.6–4.2-m range with sustained wind speeds and wind gusts of 28–33 kt (14–17 m s^{-1}) and 34–40 kt (18–21 m s^{-1}),

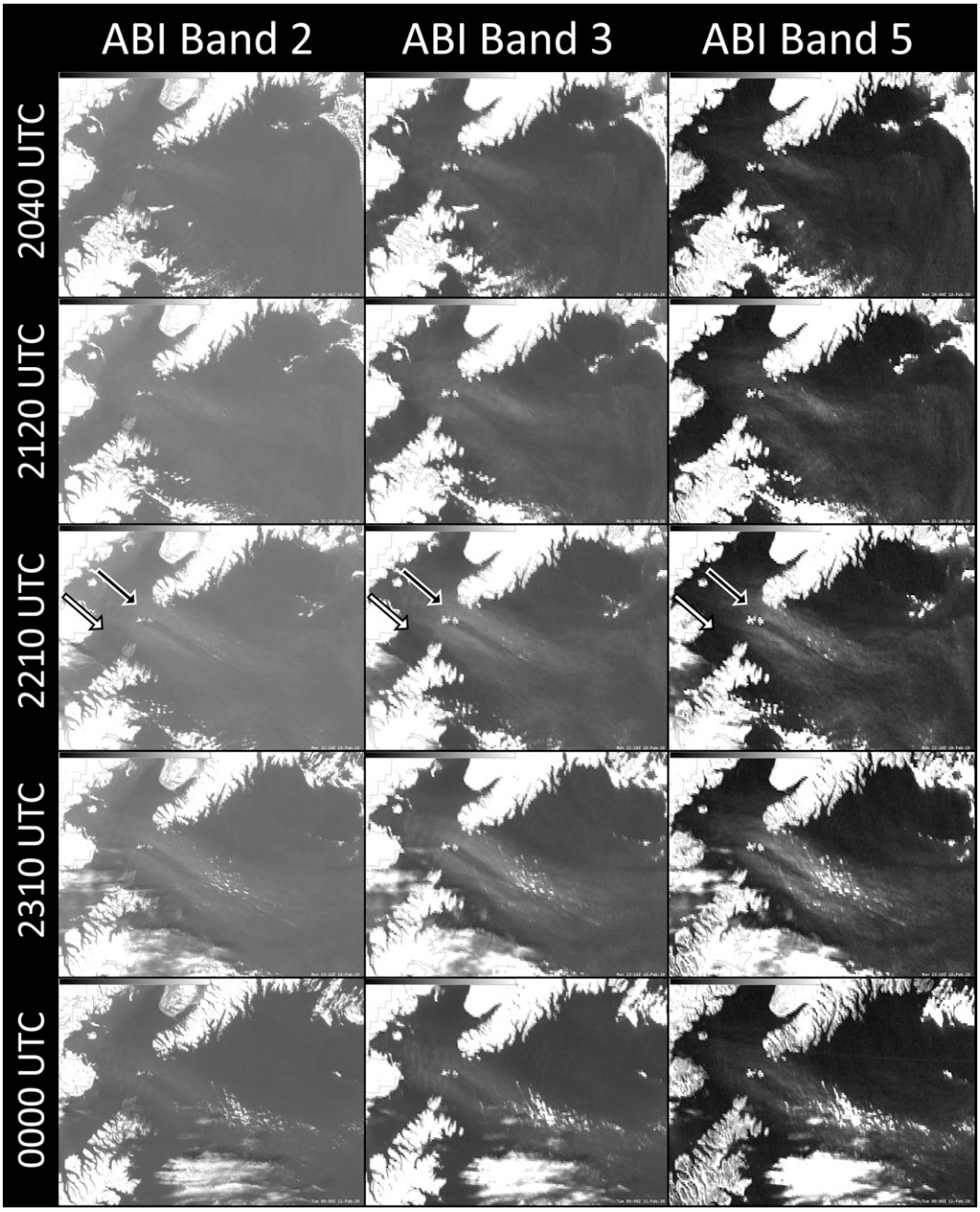

FIG. 11. The 2040, 2120, 2210, and 2310 UTC 10 Feb and 0000 UTC 11 Feb 2020 (shown from top to bottom) GOES-West ABI bands (left) 2, (center) 3, and (right) 5 (see text for wavelength associations). All products utilize a linear grayscale color table, with increasing reflectance represented by increasingly lighter shades of gray. Arrows point to areas of sea spray (black with white outline) and non–sea spray (white with black outline).

respectively. The air temperature at the buoy ranged from 2.0° to −1.0°C, and the water temperature was from 5.0° to 4.7°C. The combination of gusty winds, cold air and sea surface temperatures, and rough seas confirmed conditions were conducive for the development of freezing spray per previous studies referenced in section 1. Specifically, using the Overland (1990) technique, observed conditions within Cook Inlet fell well within the "moderate" icing class during the day, and would advance into the "heavy" icing class during periods of strong wind gusts.

Local webcams confirmed the presence of whitecaps and hazy conditions from sea spray on 10 February 2020. A webcam at Nanwalek facing west across western Cook Inlet toward Augustine Island reveals increasing and abundant

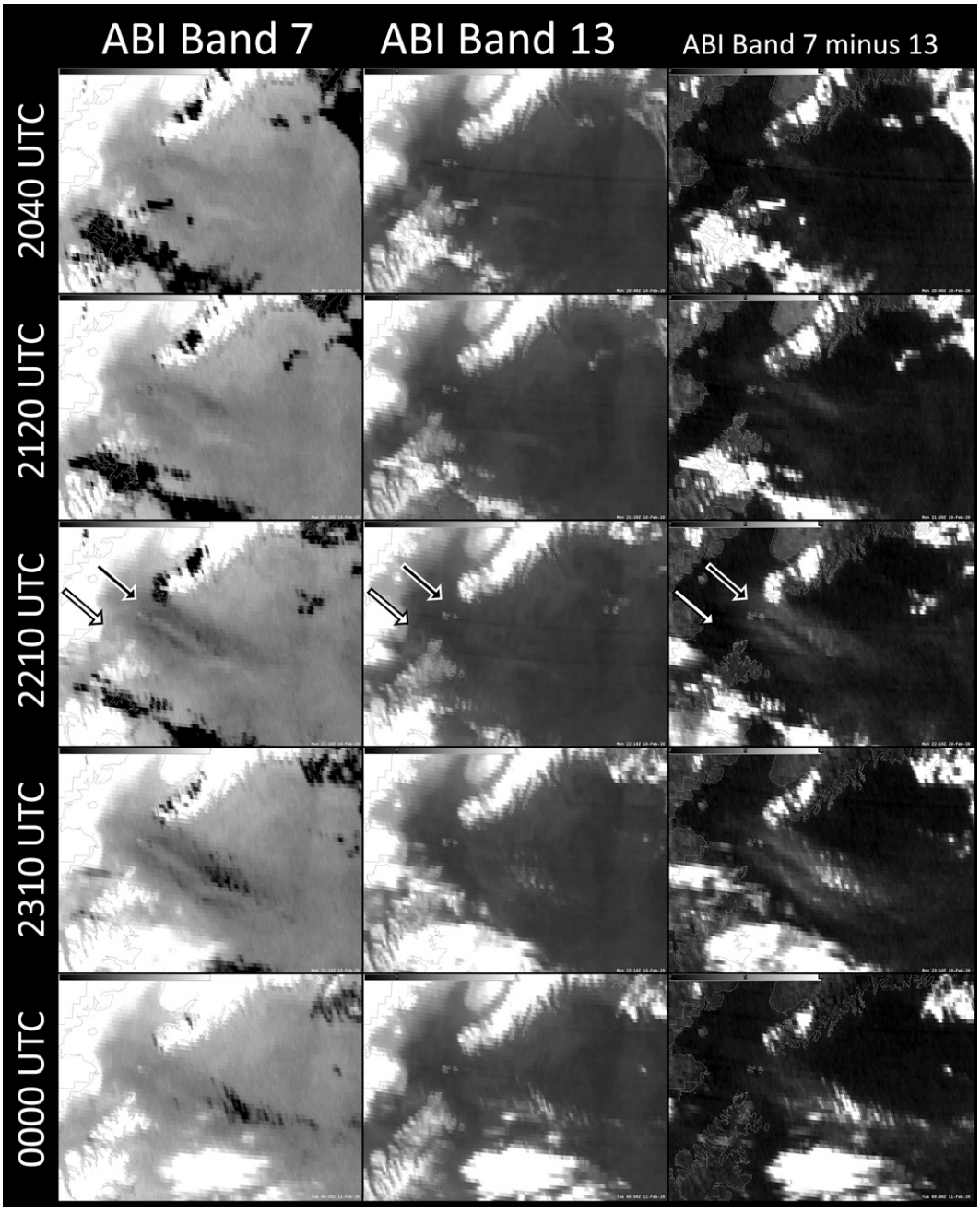

FIG. 12. The 2040, 2120, 2210, and 2310 UTC 10 Feb and 0000 UTC 11 Feb 2020 (shown from top to bottom) GOES-West ABI (left) band 7, (center) band 13, and (right) band 7 minus 13 difference (see text for wavelength associations). All products utilize a linear grayscale color table, with decreasing brightness temperature/increasing difference represented by increasingly lighter shades of gray. Arrows point to areas of sea spray (black with white outline) and non–sea spray (white with black outline).

white cap activity and boundary layer haze within the field of view throughout the day (Fig. 6). Additionally, Augustine Island becomes progressively masked during the day, implying the presence of haze immediately above the ocean surface.

Given the relatively high latitude of the viewing region of interest, five VIIRS passes (three from *NOAA-20*, two from *Suomi NPP*) were available during the day within a 3.5-h period. The first three 375-m VIIRS I bands (VIS, NIR1, NIR2) for each of the five passes are shown in Fig. 7, centered over Cook Inlet and western GoA. A sea spray signature is apparent in each of the displays, extending southeast through Cook Inlet and out into the broader GoA, as a swath of

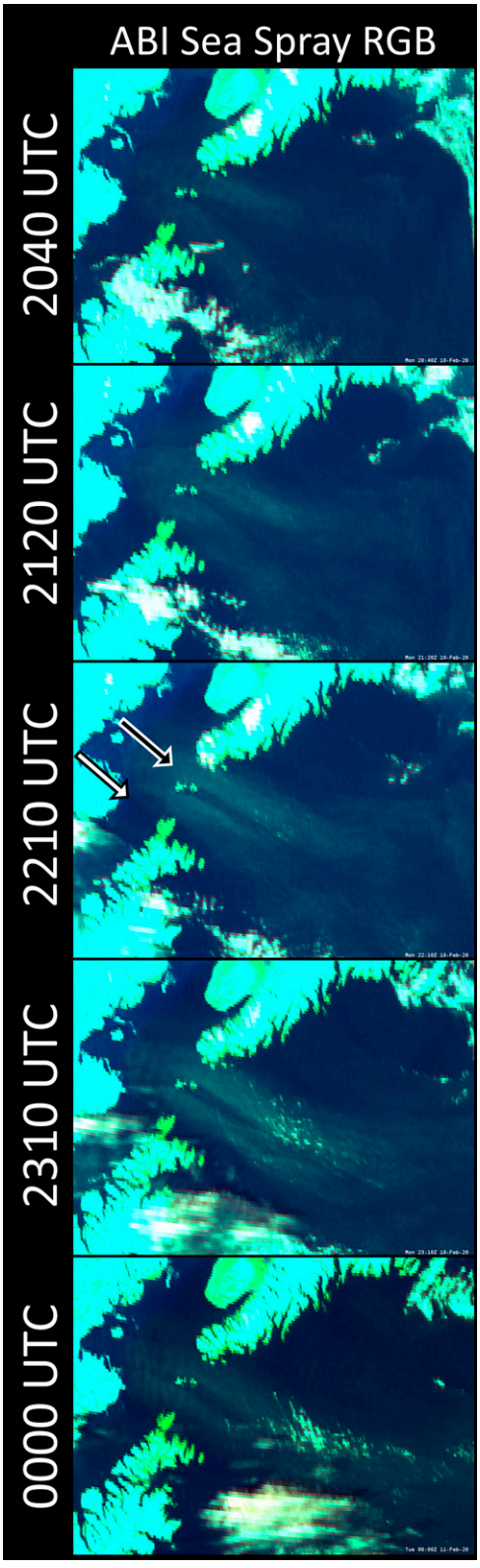

FIG. 13. The 2040, 2120, 2210, and 2310 UTC 10 Feb and 0000 UTC 11 Feb 2020 GOES-West ABI sea spray RGB (shown from top to bottom). Details about the sea spray RGB can be found in the text. Arrows point to areas of sea spray (black with white outline) and non–sea spray (white with black outline).

relatively higher reflectance compared to surrounding waters, or medium shades of gray. The 375-m VIIRS I band SWIR, IRW, and SWIR minus IRW difference are compared in Fig. 8. In the SWIR band, the signature exhibits a slightly warmer brightness temperature (darker shade of gray) compared to other areas due to the extra contribution of scattering by SSA. Analysis of the IRW band reveals no sea spray signature. Given the sea spray signature is noticeable in the VIS, NIR, NIR2, and SWIR bands, but absent in the IRW band, the signature at hand is very near the surface and/or is transparent to longwave infrared radiation. Differencing SWIR with IRW bands, sea spray areas have relatively high positive values (lighter shades of gray), confirming the detection of sea spray in the SWIR band is primarily due to the increased scattering of solar radiation in these regions of sea spray.

Additional multispectral imagery products help to further isolate the sea spray signature. The sea spray RGB isolates regions of sea spray as medium cyan to gray, compared to the dark cyan of the clear and calm ocean surface, green to bright cyan of the land surface, and white of clouds (Fig. 9). The sea spray signature appears as a relatively light shade of cyan compared to that of the non–sea spray waters due to the combined contributions of relatively high reflectance in the VIS and NIR1 bands, and greater SWIR-IRW. Turbid waters along the coast appear closer to true blue. The value of the sea spray RGB over previously shown imagery and products is that it takes beneficial characteristics of the individual bands and combines them into a single product in order to best isolate sea spray from other features.

Interestingly, alternating bands of higher and lower reflectance are diagnosed embedded within the region of sea spray, perhaps signifying relative lulls in sea spray activity. These features are captured, to an extent, in the HRRR analysis imagery already shown. A cause may be broad gravity wave features, induced by the upstream terrain, trapped within a low-level stable layer acting to cause alternating periods of active and less active strong surface winds and resulting sea spray production. Additionally, a notable lack of sea spray signature is present downstream of the Ushagat and Amatuli Islands and Mount Douglas and Fourpeaked Mountain, likely due to blocking of gusty winds by the terrain.

A Sentinel-2 swath was available over the western half of Cook Inlet at 2149 UTC, between the timestamps of the second and third VIIRS swaths. The 10-m true color imagery confirms the presence of whitecaps and sea spray within the region of suspected sea spray as observed in VIIRS (Fig. 10, top). Viewing a sector of the same size but farther south and downstream of Mount Douglas and Fourpeaked Mountain, where the sea spray signature was not as apparent in VIIRS, whitecaps and sea spray are significantly less dense spatially

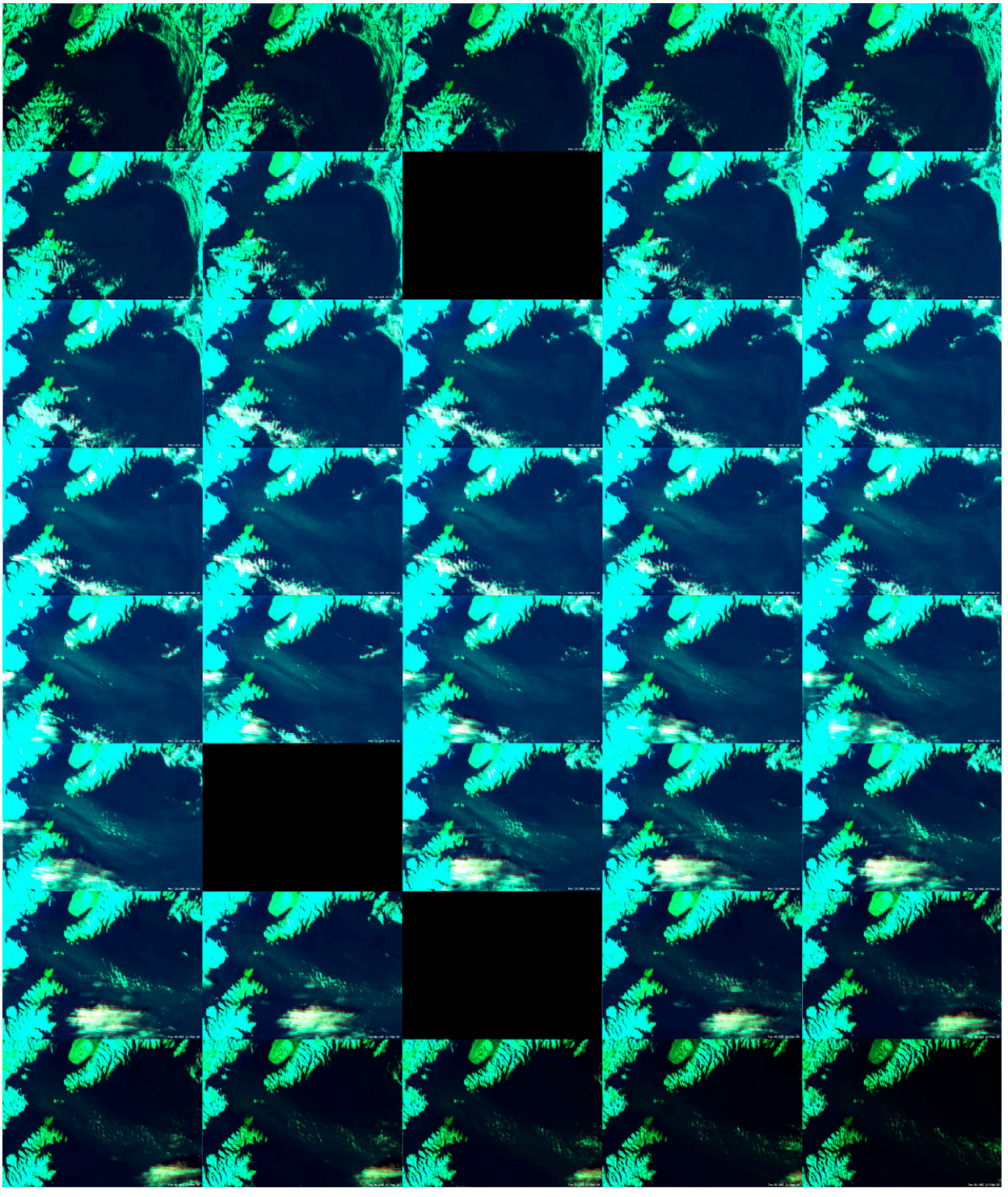

FIG. 14. The 1900 UTC 10 Feb 2020–0140 UTC 11 Feb 2020 (from left to right and from top to bottom) GOES-West ABI full disk sector sea spray RGB (this sequence of images is available as an animation in the online supplemental material: video 1).

or not apparent at all, and the overall scene lacks the haziness of sea spray (Fig. 10, bottom).

A comparison of GOES-West ABI bands, band difference, and sea spray RGB, corresponding to the VIIRS bands/products, is presented in Figs. 11–13. The times were chosen to allow for comparison with the VIIRS imagery. The sea spray is apparent in the ABI imagery, to varying degrees, similar to in VIIRS imagery. Of course, the level of detail

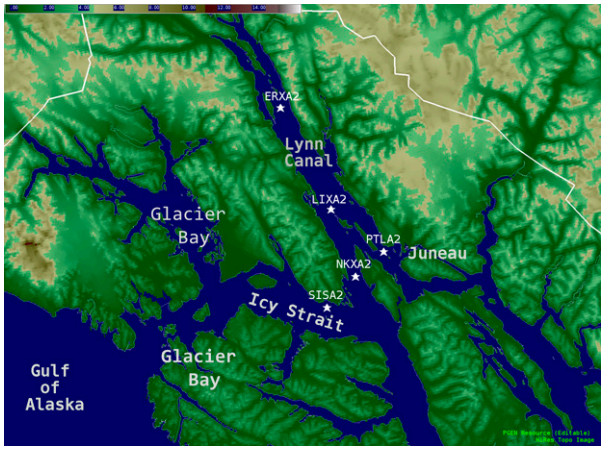

FIG. 15. Region of interest for 5 Mar 2020 sea spray case. Relevant geographic landmarks (gray) and locations of C-Man stations and buoys (white) are labeled.

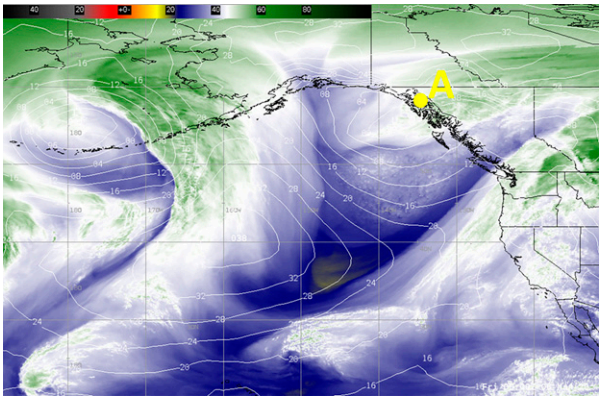

FIG. 16. The 0000 UTC 6 Mar 2020 GOES-West 6.2-μm water vapor imagery (color fill) and GFS mean sea level pressure analysis (hPa; white contours). Point A refers to the region of interest for this case.

apparent in the ABI imagery is significantly less due to lower spatial resolution nominally, and significant distance from the satellite sub-point. The coarser resolution is most impactful along the edge of the sea spray plume, where the signature becomes fainter, and along the coasts. This is especially noticeable with the lower, 2-km, resolution SWIR and IRW bands, and resulting SWIR-IRW. The sea spray detection capabilities are diminished in the VIS band compared to the NIR1 and NIR2 bands for reasons outlined in section 3. However, the added detail of the VIS given its higher spatial resolution compared to the other ABI bands makes it worthwhile in the sea spray analysis. The locations experiencing sea spray again appear as relatively higher reflectance in the VIS and NIR bands, warmer brightness temperature in the SWIR band, and positive values in the SWIR-IRW.

The sea spray RGB is applied to the ABI bands, and similarly isolates the sea spray signature as medium cyan to gray, but with reduced spatial detail. The inclusion of the 0.5-km VIS band helps to maintain some of the spatial detail that is lost in the lower resolution NIR2 band and SWIR-IRW.

The high temporal resolution of GOES ABI gives it an advantage over other data sources, such as VIIRS, in detecting and tracking sea spray with time. Specifically, the presence of sea spray becomes most obvious when viewing an animation of images versus viewing each image alone. In a daytime (1800–0200 UTC) animation of ABI sea spray RGB images captured every 10 min, the region of apparent sea spray appears to spread downwind along with the progression of the strongest wind gusts as was detailed in the HRRR analyses (Fig. 14). The appearance of sea spray becomes most obvious during the middle of the day, likely due to a combination of highest sun angle and strongest surface wind gusts. As long as one is confident that they have diagnosed sea spray in a given area, GOES imagery is the ideal data source for tracking the evolution of sea spray with time.

b. 5 March 2020 southeast Alaska inner channel case study

A similar synoptic setup to that on 10 February 2020 led to gusty winds and sea spray through the inner channels of southeast Alaska on 5 March 2020 (Fig. 15). GOES-West Water Vapor imagery depicted a shortwave trough exiting the GoA into southeast Alaska, while another trough progressed east over the Aleutians (Fig. 16). Corresponding surface analysis from the GFS model captured a surface low with a tight pressure gradient centered over southeast Alaska. Given the anticipated cold and windy conditions, the Juneau, Alaska, NWS WFO issued a CWF at 0426 LT that included a heavy

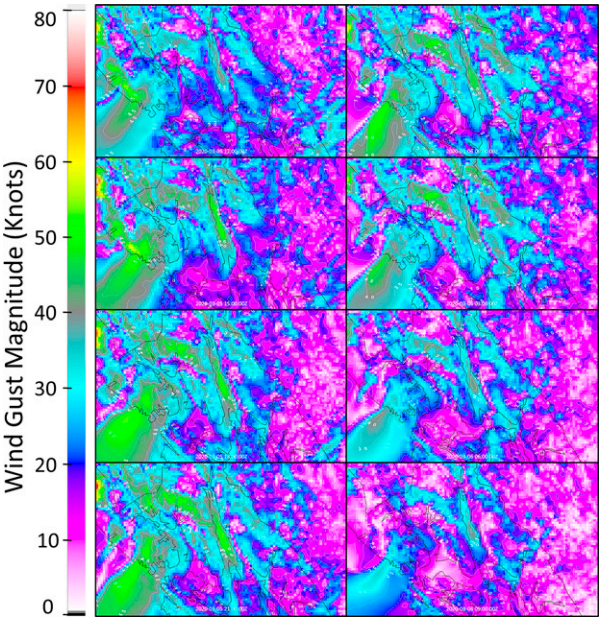

FIG. 17. The 1200 UTC 5 Mar–0900 UTC 6 Mar 2020 NCEP/HRRR 3-hourly (shown from top to bottom and from left to right) wind gust (kt) analysis fields (fill and contour).

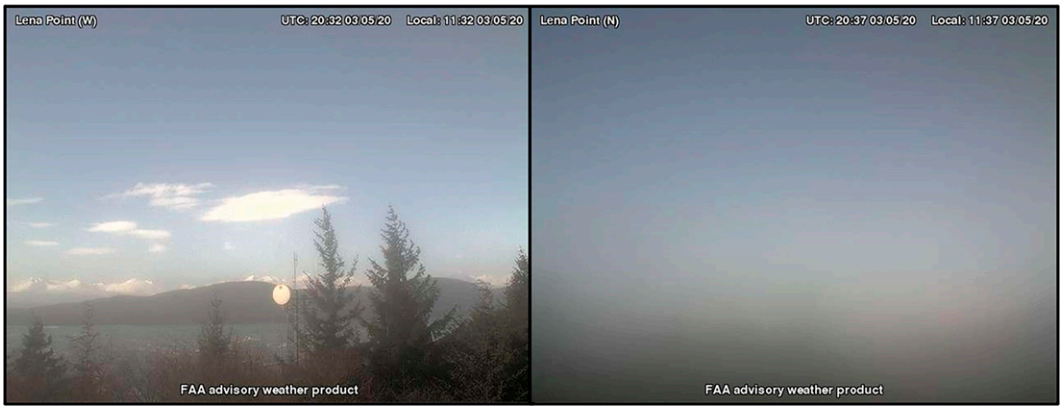

FIG. 18. The (left) 2032 UTC west-facing and (right) 2037 UTC north-facing FAA webcam at Lena Point (6 km north of PTLA2) viewing into Favorite Channel.

freezing spray warning for Lynn Canal to go along with 40–55 kt (21–28 m s^{-1}) North winds and wave heights to 10 ft (3 m).

Strong wind gusts did develop across the inner channels of southeast Alaska during the day/evening of 5 March 2020. The HRRR model analyzed winds gusting in excess of 50 kt (26 m s^{-1}) across Lynn Canal during the afternoon of 5 March (Fig. 17). Wind gusts remained less than 20 kt (10 m s^{-1}) across Icy Strait, where north winds are blocked by terrain.

C-MAN and Fixed Structure Weather Stations confirmed gusty winds developing across Lynn Canal from the late-night hours on 4 March through the morning hours on 6 March. Sustained wind speeds and wind gusts of 38–48 kt (20–25 m s^{-1}) and 49–71 kt (25–37 m s^{-1}), respectively, were observed at ERXA2 and LIXA2, while measurements of 31–45 kt (16–23 m s^{-1}) and 46–67 kt (24–34 m s^{-1}), respectively, were taken farther south at PTLA2 and NKXA2, during the daytime period of 1600 and 0100 UTC. Air temperatures across Lynn Canal dropped from −1.4°C to as low as −5.8°C during the daytime hours. The gusty winds and cold air temperatures meant meteorological conditions were conducive for the development of freezing sea spray across Lynn Canal. Meanwhile in Icy Strait at SISA2, wind speeds and wind gusts remained less than 15 kt (8 m s^{-1}) and 26 kt (13 m s^{-1}), respectively, during the same period. Once again using the Overland (1990) technique, observed conditions within Lynn Canal fell within the "moderate" icing class, and approached "heavy" during periods of cooler air temperatures and gusting winds.

A webcam at Lena Point (6 km north of PTLA2) looking west into southern Favorite Channel (located immediately southeast of Lynn Canal, along the east side of Shelter Island southeast of LIXA2 and PTLA2) captured whitecaps as well as sea spray haze throughout the afternoon (Fig. 18). The north pointing view from the same location (sensing into the wind) was almost completely obstructed by aerosols blowing into the camera. A photo taken by one of the coauthors looking west into Favorite Channel during the day confirmed the presence of abundant whitecaps and hazy conditions due to sea spray (Fig. 19).

FIG. 19. Photo taken looking west into Favorite Channel from west Juneau, AK. Location of the photographer is marked as a yellow circle in the inset image. (Photo credit: Carl Dierking.)

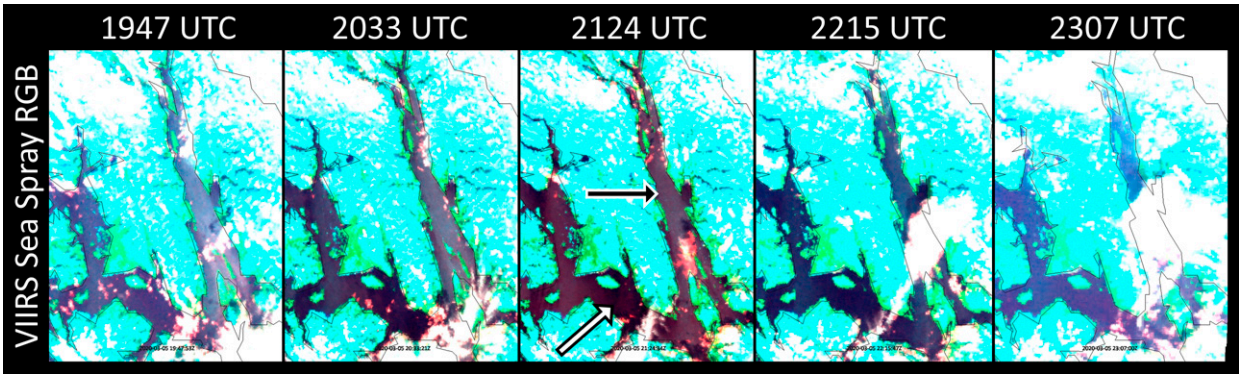

FIG. 20. The 1947, 2033, 2124, 2215, and 2307 UTC 5 Mar 2020 *NOAA-20* and *SNPP* VIIRS sea spray RGB (shown from left to right). Details about the sea spray RGB can be found in the text. Arrows point to areas of sea spray (black with white outline) and non–sea spray (white with black outline).

Similar to the previous case, five VIIRS passes were available over southeast Alaska during the early afternoon (three from *NOAA-20*, two from *SNPP*). The sea spray RGB again exhibits a clear signal of medium cyan to gray colors within Lynn Canal, where sea spray was suspected given favorable environmental conditions (Fig. 20). Alternatively, the RGB exhibits an obviously darker shade of cyan within Icy Strait, where wind speeds were less conducive for sea spray.

A Sentinel-2 pass was available over the Juneau area at 2038 UTC 5 March (Fig. 21). Whitecaps and sea spray haziness fill the scene across Lynn Canal, while waters are calm and haze absent over Icy Strait, corroborating the VIIRS imagery analysis.

Compared to the VIIRS imagery, the coarser resolution of the ABI imagery is especially noticeable with this small-scale event (Fig. 22). The exact edge of sea spray extent, especially near the coasts, is less obvious to undetectable. Areas characterized by a faint sea spray signature, such as across Glacier Bay, are also less apparent in the ABI imagery compared to in the VIIRS imagery. In general, however, sea spray does remain apparent across Lynn Canal when analyzing the ABI imagery. The signature appears as a relatively lighter shade of cyan compared to the non–sea spray region of Icy Strait. The inclusion of the higher resolution 500-m VIS in the RGB, when the other ingredients are 1- and 2-km resolution, is particularly valuable in helping to diagnose the sea spray signature with smaller-scale events such as this one.

Taking advantage of the ABI temporal resolution and putting the imagery in motion, the signal appears to grow during the morning and peak around 2100 UTC, before decreasing again in intensity (Fig. 23). While this assessment matches wind speed trends diagnosed in HRRR analyses and surface

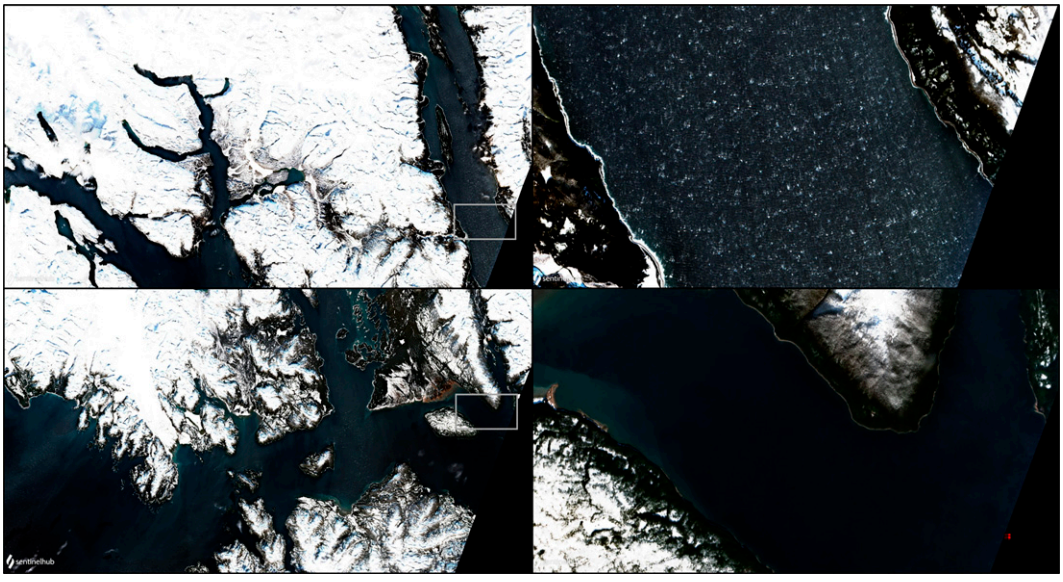

FIG. 21. The 2038 UTC 5 Mar 2020 Sentinel-2 true color imagery. Imagery includes portions of (top) Lynn Canal and (bottom) Icy Strait. The gray rectangles in the left images denote the zoomed in regions of the right images.

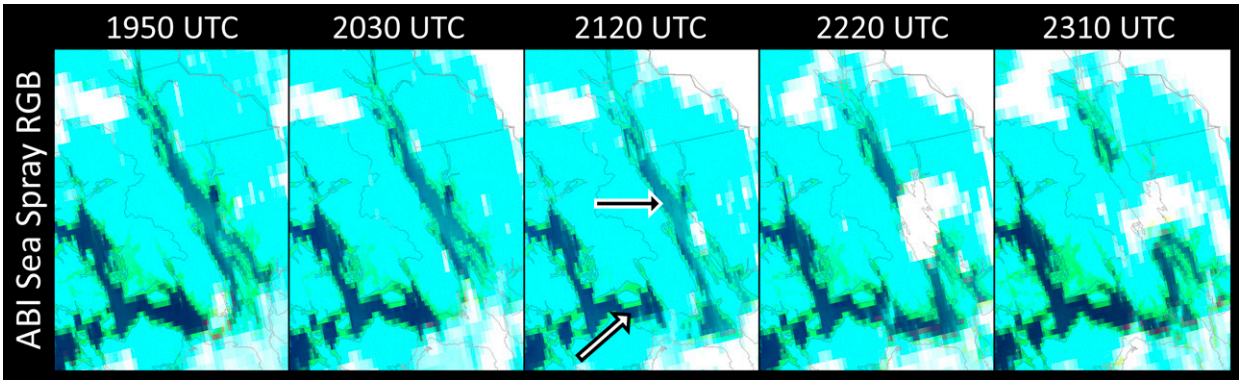

FIG. 22. The 1950, 2030, 2120, 2220, and 2310 UTC 5 Mar 2020 GOES-West ABI sea spray RGB (shown from left to right). Details about the sea spray RGB can be found in the text. Arrows point to areas of sea spray (black with white outline) and non–sea spray (white with black outline).

observations, it is also likely due, in part, to evolving reflectance patterns due to sun angle changes. However, if one acknowledges reflectance trends of the overall scene due to changes in sun angle, it is apparent that there is a unique signal and trend within the sea spray region compared to the less windy areas.

5. Discussion

The previous section highlighted GOES ABI and JPSS VIIRS capabilities for detecting areas of sea spray. Given the considerable impacts of freezing spray on life and property, the NWS includes mention of freezing spray in their CWF. Further, a heavy freezing spray warning will be issued under exceptional conditions. These forecasts are primarily automated and based on model forecasts of environmental conditions. Given a lack of observations, forecasts of freezing spray are rarely verified. NWS forecasters also communicate freezing spray potential to inquiring mariners as a form of IDSS. The information provided is largely based on model data and limited observations.

Freezing spray conditions are fairly common across Alaska coastal waters regions, according to NWS forecasts. Figure 24 illustrates the number of freezing spray days in NWS Anchorage and NWS Juneau forecasts between 2011 and 2020, by month. Freezing spray events occurred during the months of October–May, and developed almost every day from December–March within the NWS Anchorage forecast area. In their morning forecast packages, NWS Anchorage (Juneau) included freezing spray in the CWF 161.5 (39.3) days yr^{-1}, and issued a heavy freezing spray warning 84.8 (12.3) days yr^{-1}, on average.

Additional observations of sea spray occurring in the right environmental conditions would be beneficial to forecasters and mariners in several ways. At least a subset of freezing spray forecasts could be verified, leading to better forecast calibration and improved overall forecasts of freezing spray in the long term. In the short term, mentions of freezing spray could be added to or removed from the forecast given the observation, or lack thereof, in satellite imagery. Further, IDSS related to freezing spray is improved using these techniques as inquiring mariners could be given more concrete information regarding ongoing and developing regions of sea spray. Images and animations of sea spray could also be disseminated via social media and other public/partner communication pathways in an effort to raise awareness to the hazard.

The marine community, if equipped with the right tools, could also be trained on the detection of sea spray via satellite imagery, allowing them to make more informed operational decisions.

6. Summary and conclusions

Freezing spray poses a significant hazard to marine vessels, especially at high latitudes. The accumulation of freezing spray can and has caused marine vessels to capsize, resulting in loss of life and property. The NWS generates largely automated forecasts of freezing spray, with little verification. NWS forecasters also provide IDSS to inquiring mariners regarding freezing spray potential. Unfortunately, given a sparse observation network, detection of sea spray and verification of freezing spray forecasts are rare.

This paper introduced previously underutilized oceanic sea spray detection techniques using NOAA GOES ABI and JPSS VIIRS imagery already available to forecasters in operational AWIPS-II. While VIIRS provides the spatial resolution to better diagnose smaller-scale events, sea spray area boundaries, and sea spray among non-overcast cloud cover, ABI allows for the user to better track the evolution of sea spray in time given the relatively high temporal resolution. Animations of GOES and VIIRS imagery allow for the sea spray feature to be more easily diagnosed versus the viewing of single images alone. By using operational satellite imagery to detect the presence of sea spray, forecasters can improve forecasts of areas of potential freezing spray, and improve IDSS related to freezing spray.

Immediate next steps will be to share color tables, RGBs, and procedures, developed as a result of this work, with relevant NWS offices. Continued interaction with current and

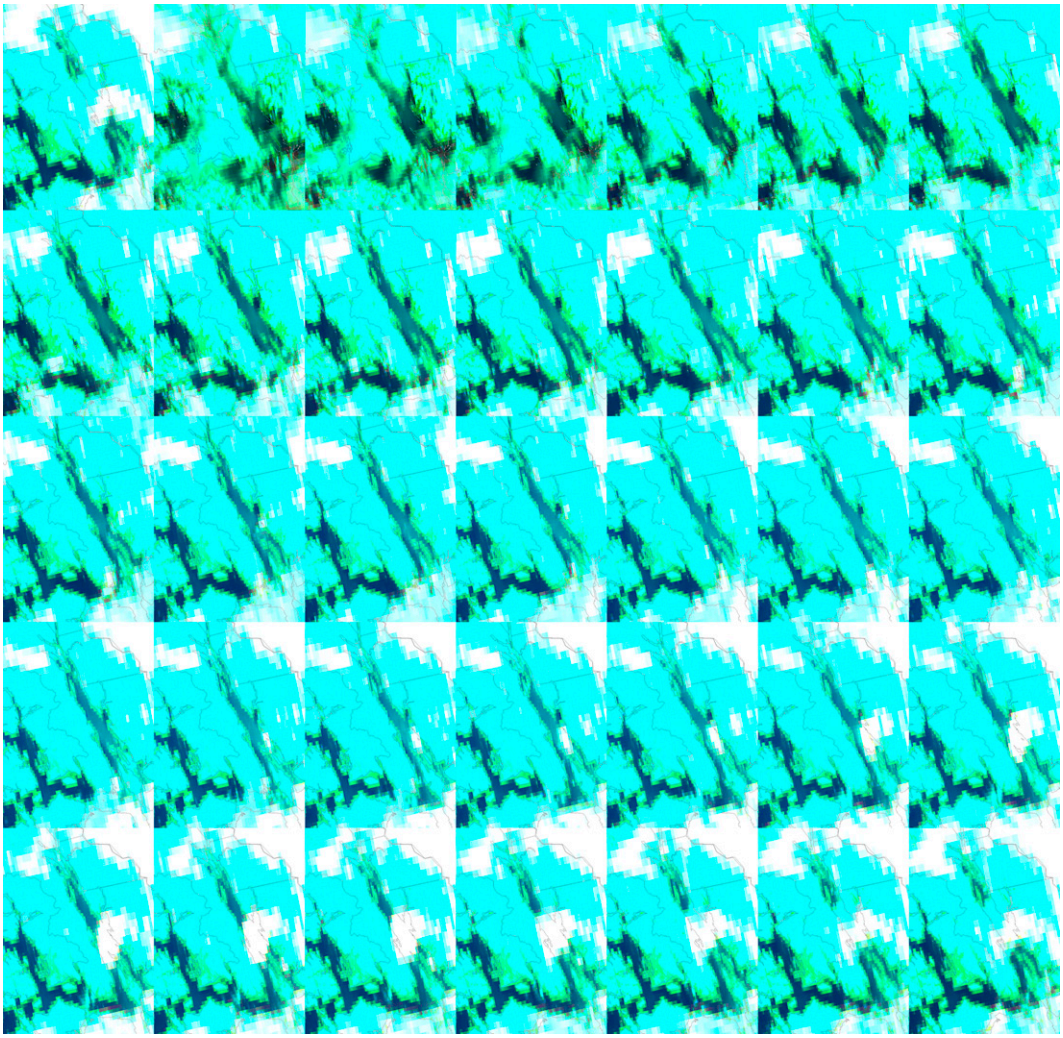

FIG. 23. The 1730–2320 UTC 5 Mar 2020 (shown from left to right and from top to bottom) GOES-West ABI full disk sector sea spray RGB (this sequence of images is available as an animation in the online supplemental material: video 2).

additional NWS collaborators will result in further feedback, potentially leading to adjustments and improvements in detection techniques using imagery from NOAA satellites. Given the novelty of the sea spray detection technique, and occasional subtlety of the sea spray signature, training will need to be developed and delivered to forecasters. Considering operational time constraints, training in the form of quick guides, blog post examples, and brief live interactions with local satellite focal points will be ideal.

There are a number of future studies that could stem from this initial look at clear-sky sea spray detection using operational NOAA weather satellites. As was discussed throughout the paper, forecasts of freezing spray could be verified against its occurrence as observed in satellite imagery. Automation of the sea spray detection technique, and therefore, the sea spray forecast verification as well, is a logical next step. Over time, a climatology of sea spray events across the GoA and adjacent inner channels could be established. From the climatology, composite maps and guidelines relating the occurrence of sea spray with specific synoptic setups may be generated. Additionally, investigations could be initiated looking into whether the presence of a satellite sea spray signature and its apparent severity could be tied to a surface wind speed threshold. From this, one could verify short-term model guidance of wind speeds. Continuing, the sea spray satellite signature could be combined with other NOAA satellite products, such as those that convey information about sea surface temperature and wind speed, to provide a likelihood of ongoing sea spray and freezing spray. Finally, detection of sea spray at night using NOAA satellite imagery, either infrared or low light imagery, is worthwhile.

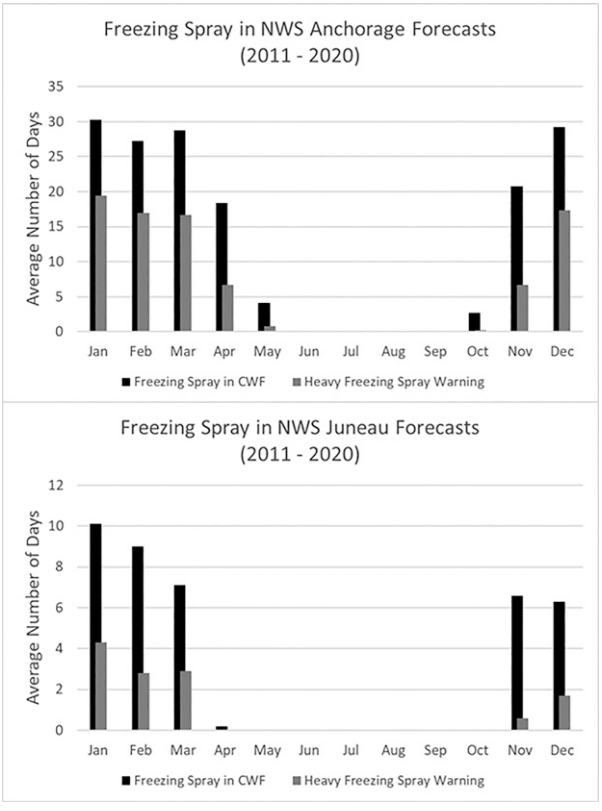

FIG. 24. The 2011–20 (top) NWS Anchorage and (bottom) NWS Juneau average number of days with freezing spray in the morning CWF, and average number of days with a heavy freezing spray warning, by month.

Acknowledgments. This work was supported by the National Oceanic and Atmospheric Administration (Grant NA19OAR4320073). Sentinel-2 imagery was provided by the ESA through the Sentinel-Hub EO Browser (https://apps.sentinel-hub.com/eo-browser/). Archived NWS text forecast products were accessed from the Iowa State University, Iowa Environmental Mesonet webpage (https://mesonet.agron.iastate.edu/). FAA webcam images were accessed from the FAA WeatherCams webpage (https://weathercams.faa.gov). SCATSAT, ASCAT, and AMSR-2 data were accessed from the STAR Ocean Surface Winds Team webpage (https://manati.star.nesdis.noaa.gov/datasets/ASCATData.php). Buoy and C-MAN station data were accessed from the NOAA National Data Buoy Center (https://www.ndbc.noaa.gov/). Disclaimer: The views, opinions, and findings contained in this article are those of the authors and should not be construed as an official National Oceanic and Atmospheric Administration (NOAA) or U.S. government position, policy, or decision.

REFERENCES

Achtor, T., T. Rink, R. Whittaker, D. Parker, and D. Santek, 2008: McIDAS-V: A powerful data analysis and visualization tool for multi and hyperspectral environmental satellite data. *Proc. SPIE*, **7085**, 708509, https://doi.org/10.1117/12.795223.

Andreas, E. L, and J. DeCosmo, 1999: Sea spray production and influence on air–sea heat and moisture fluxes over the open ocean. *Air–Sea Exchange: Physics, Chemistry and Dynamics*, G. L. Geernaert, Ed., Springer, 327–362, https://doi.org/10.1007/978-94-015-9291-8_13.

——, and K. A. Emanuel, 2001: Effects of sea spray on tropical cyclone intensity. *J. Atmos. Sci.*, **58**, 3741–3751, https://doi.org/10.1175/1520-0469(2001)058<3741:EOSSOT>2.0.CO;2.

——, J. B. Edson, E. C. Monahan, M. P. Rouault, and S. D. Smith, 1995: The spray contribution to net evaporation from the sea: A review of recent progress. *Bound.-Layer Meteor.*, **72**, 3–52, https://doi.org/10.1007/BF00712389.

Anguelova, M. D., and F. Webster, 2006: Whitecap coverage from satellite measurements: A first step toward modeling the variability of oceanic whitecaps. *J. Geophys. Res.*, **111**, C03017, https://doi.org/10.1029/2005JC003158.

Blanchard, D., 1983: The production, distribution, and bacterial enrichment of the sea-salt aerosol. *Air-Sea Exchange of Gases and Particles*, P. S. Liss and W. G. N. Slinn, Eds., Springer, 407–454, https://doi.org/10.1007/978-94-009-7169-1_7.

Dehghani-Sanij, A. R., S. R. Dehghani, G. F. Naterer, and Y. S. Muzychka, 2017: Sea spray icing phenomena on marine vessels and offshore structures: Review and formulation. *Ocean Eng.*, **132**, 25–39, https://doi.org/10.1016/j.oceaneng.2017.01.016.

De Leeuw, G., E. L Andreas, M. D. Anguelova, C. W. Fairall, E. R. Lewis, C. O'Dowd, M. Schulz, and S. E. Schwartz, 2011: Production flux of sea spray aerosol. *Rev. Geophys.*, **49**, RG2001, https://doi.org/10.1029/2010RG000349.

Drusch, M., and Coauthors, 2012: Sentinel-2: ESA's optical high-resolution mission for GMES operational services. *Remote Sensing Environ.*, **120**, 25–36, https://doi.org/10.1016/j.rse.2011.11.026.

Elsenheimer, C. B., and C. M. Gravelle, 2019: Introducing lightning threat messaging using the *GOES-16* day cloud phase distinction RGB composite. *Wea. Forecasting*, **34**, 1587–1600, https://doi.org/10.1175/WAF-D-19-0049.1.

EUMETSAT User Services, 2009: Best practices for RGB compositing of multi-spectral imagery. European Organisation for the Exploitation of Meteorological Satellites, 8 pp., https://www-cdn.eumetsat.int/files/2020-04/pdf_using_rgb_best_practices.pdf.

Fairall, C. W., J. D. Kepert, and G. J. Holland, 1994: The effect of sea spray on surface energy transports over the ocean. *Global Atmos. Ocean Syst.*, **2**, 121–142.

Gall, J. S., W. M. Frank, and Y. Kwon, 2008: Effects of sea spray on tropical cyclones simulated under idealized conditions. *Mon. Wea. Rev.*, **136**, 1686–1705, https://doi.org/10.1175/2007MWR2183.1.

Goldberg, M. D., H. Kilcoyne, H. Cikanek, and A. Metha, 2013: Joint Polar Satellite System: The United States next generation civilian polar-orbiting environmental satellite system. *J. Geophys. Res. Atmos.*, **118**, 13 463–13 475, https://doi.org/10.1002/2013JD020389.

Guest, P., and R. Luke, 2005: Vessel icing. *Mar. Wea. Log*, **49** (3), https://www.vos.noaa.gov/MWL/dec_05/ves.shtml.

Hillger, D., and Coauthors, 2013: First-light imagery from *Suomi NPP* VIIRS. *Bull. Amer. Meteor. Soc.*, **94**, 1019–1029, https://doi.org/10.1175/BAMS-D-12-00097.1.

Jones, K. F., and E. L Andreas, 2012: Sea spray concentrations and the icing of fixed offshore structures. *Quart. J. Roy. Meteor. Soc.*, **138**, 131–144, https://doi.org/10.1002/qj.897.

Lindley, T. T., A. R. Anderson, V. N. Mahale, T. S. Curl, W. E. Line, S. S. Lindstrom, and A. S. Bachmeier, 2016: Wildfire detection notifications for impact-based decision support services in Oklahoma using geostationary super rapid scan satellite imagery. *J. Oper. Meteor.*, **4**, 182–191, https://doi.org/10.15191/nwajom.2016.0414.

Line, W. E., T. J. Schmit, D. T. Lindsey, and S. J. Goodman, 2016: Use of geostationary super rapid scan satellite imagery by the Storm Prediction Center. *Wea. Forecasting*, **31**, 483–494, https://doi.org/10.1175/WAF-D-15-0135.1.

Liu, H., P. Q. Olsson, K. P. Volz, and H. Yi, 2006: A climatology of mesoscale model simulated low-level wind jets over Cook Inlet and Shelikof Strait, Alaska. *Estuarine Coastal Shelf Sci.*, **70**, 551–566, https://doi.org/10.1016/j.ecss.2006.06.011.

Lozowski, E. P., K. Szilder, and L. Makkonen, 2000: Computer simulation of marine ice accretion. *Philos. Trans. Roy. Soc. London*, **A358**, 2811–2845, https://doi.org/10.1098/rsta.2000.0687.

Macklin, S. A., N. A. Bond, and J. P. Walker, 1990: Structure of a low-level jet over lower Cook Inlet, Alaska. *Mon. Wea. Rev.*, **118**, 2568–2578, https://doi.org/10.1175/1520-0493(1990)118<2568:SOALLJ>2.0.CO;2.

Makkonen, L., R. D. Brown, and P. T. Mitten, 1991: Comments on "Prediction of vessel icing for near-freezing sea temperatures." *Wea. Forecasting*, **6**, 565–567, https://doi.org/10.1175/1520-0434(1991)006<0565:COOVIF>2.0.CO;2.

Meirink, J. F., and V. K. Makin, 2001: The impact of sea spray evaporation in a numerical weather prediction model. *J. Atmos. Sci.*, **58**, 3626–3638, https://doi.org/10.1175/1520-0469(2001)058<3626:TIOSSE>2.0.CO;2.

Moore, K., 2020: Scandies Rose: Sinking marks grim start to 2020. *National Fisherman*, 5 February, https://www.nationalfisherman.com/alaska/scandies-rose-sinking-marks-grim-start-to-2020.

NWS, 2020: National Weather Service Glossary. NWS, accessed 1 May 2020, https://w1.weather.gov/glossary/.

Ortiz-Suslow, D. G., B. K. Haus, S. Mehta, and N. M. Laxague, 2016: Sea spray generation in very high winds. *J. Atmos. Sci.*, **73**, 3975–3995, https://doi.org/10.1175/JAS-D-15-0249.1.

Overland, J. E., 1990: Prediction of vessel icing for near-freezing sea temperatures. *Wea. Forecasting*, **5**, 62–77, https://doi.org/10.1175/1520-0434(1990)005<0062:POVIFN>2.0.CO;2.

——, C. H. Pease, R. W. Preisendorfer, and A. L. Comiskey, 1986: Prediction of vessel icing. *J. Climate Appl. Meteor.*, **25**, 1793–1806, https://doi.org/10.1175/1520-0450(1986)025<1793:POVI>2.0.CO;2.

Panov, V. V., 1978: Icing of ships. *Polar Geogr.*, **2**, 166–186, https://doi.org/10.1080/10889377809388652.

Perrie, W., E. L Andreas, W. Zhang, W. Li, J. Gyakum, and R. McTaggart-Cowan, 2005: Sea spray impacts on intensifying midlatitude cyclones. *J. Atmos. Sci.*, **62**, 1867–1883, https://doi.org/10.1175/JAS3436.1.

Rastigejev, Y., and S. A. Suslov, 2014: E–ε model of spray-laden near-sea atmospheric layer in high wind conditions. *J. Phys. Oceanogr.*, **44**, 742–763, https://doi.org/10.1175/JPO-D-12-0195.1.

Riehl, H., 1954: *Tropical Meteorology*. McGraw-Hill, 392 pp.

Salisbury, D. J., M. D. Anguelova, and I. M. Brooks, 2013: On the variability of whitecap fraction using satellite-based observations. *J. Geophys. Res. Oceans*, **118**, 6201–6222, https://doi.org/10.1002/2013JC008797.

Samuelson, E. M., S. Løset, and K. Edvardsen, 2015: Marine icing observed on KV Nordkapp during a cold air outbreak with a developing polar low in the Barents Sea. *Proc. 23rd Int. Conf. on Port and Ocean Engineering under Arctic Conditions*, Trondheim, Norway, Port and Ocean Engineering under Arctic Conditions, https://doi.org/10.13140/RG.2.1.2678.8006.

Schmit, T. J., and M. M. Gunshor, 2020: ABI Imagery from the GOES-R Series. *The GOES-R Series*, S. J. Goodman et al., Eds., Elsevier, 23–34, https://doi.org/10.1016/B978-0-12-814327-8.00004-4.

——, P. Griffith, M. W. Gunshor, J. M. Daniels, S. J. Goodman, and W. J. Lebair, 2017: A closer look at the ABI on the GOES-R series. *Bull. Amer. Meteor. Soc.*, **98**, 681–698, https://doi.org/10.1175/BAMS-D-15-00230.1.

Shellard, H. C., 1974: The meteorological aspects of ice accretion on ships. Marine Science Affairs Rep. 10, World Meteorological Organization, 34 pp.

Wang, Y., F. D. Kepert, and G. J. Holland, 2001: The effects of sea spray evaporation on tropical cyclone boundary layer structure and intensity. *Mon. Wea. Rev.*, **129**, 2481–2500, https://doi.org/10.1175/1520-0493(2001)129<2481:TEOSSE>2.0.CO;2.

Wu, J., 1992: Bubble flux and marine aerosol spectra under various wind velocities. *J. Geophys. Res.*, **97**, 2327–2333, https://doi.org/10.1029/91JC02568.

Zhang, W., W. Perrie, and W. Li, 2006: Impacts of waves and sea spray on midlatitude storm structure and intensity. *Mon. Wea. Rev.*, **134**, 2418–2442, https://doi.org/10.1175/MWR3191.1.